Ornamental
Plant Research

ARTICLE

Open Access

https://doi.org/10.48130/opr-0025-0037
Ornamental Plant Research **2025**, 5: e041

Regulation of scape elongation through gibberellin and auxin detected by hormone metabolomic profiling in *Clivia miniata*

Yi Ji, Li Xue* and Jiajun Lei*

College of Horticulture, Shenyang Agricultural University, Shenyang 110866, China
* Corresponding authors, E-mail: lixue@syau.edu.cn; jiajunlei@syau.edu.cn

Abstract

Clivia miniata Regel is a globally prized ornamental plant with significant economic value in China, as a traditional decoration during Lunar New Year celebrations. However, its natural anthesis time in the greenhouse often fails to coincide with the Spring Festival, thereby necessitating precise control over anthesis through a better understanding of its scape elongation mechanism. Phenological observations identified four key stages (flower bud stage, CM_F; inflorescence stage, CM_I; inflorescence emergence stage, CM_E; and scape stage, CM_S) before anthesis. Observations revealed progressive elongation of parenchyma cells in the developing scape. Hormone profiling across these stages was conducted to explore the hormonal regulation of this process, identifying 60 distinct hormones, 52 of which showed significant differential expression. Among these, auxins and gibberellins (GAs) emerged as primary regulators of both scape elongation and anthesis time. Building on these insights, exogenous hormone application experiments were performed with remarkable practical outcomes. All phytohormone treatments significantly accelerated anthesis. Specifically, applying 50 mg/L indole-3-acetic acid (IAA) resulted in complete inflorescence emergence with 100% efficiency and accelerated anthesis by 14 d. The application of 150 mg/L IAA resulted in complete inflorescence emergence with 90% efficiency and accelerated anthesis by 29 d. Moreover, the application of 150 mg/L GA_3 resulted in complete inflorescence emergence with 90% efficiency and accelerated the anthesis by 25 d. The application of 200 mg/L GA_3 resulted in complete inflorescence emergence with 80% efficiency and accelerated anthesis by 35 d, demonstrating unprecedented potential for manipulating anthesis timing. These findings elucidate the physiological and molecular mechanisms underlying anthesis time in *C. miniata*.

Citation: Ji Y, Xue L, Lei J. 2025. Regulation of scape elongation through gibberellin and auxin detected by hormone metabolomic profiling in *Clivia miniata*. *Ornamental Plant Research* 5: e041 https://doi.org/10.48130/opr-0025-0037

Introduction

The transition from vegetative to reproductive growth marks a critical phase in plant development, culminating in flowering[1]. This process is strictly regulated by the integration of endogenous genetic programs and autonomous timing mechanisms with external environmental cues such as photoperiod and temperature[2,3]. In *Arabidopsis thaliana*, floral development accelerates markedly following the formation of floral primordia, driven primarily by rapid elongation[4]. Plant morphogenesis, particularly scape elongation, is governed by intricate phytohormonal networks, with gibberellin (GA) biosynthesis gradients acting as pivotal developmental regulators[5]. These gradients trigger spatiotemporally ordered transcriptional cascades that link GA signaling to epigenetic reprogramming, driving stem elongation and developmental phase transitions[6]. The conservation of GA signaling across plant lineages is well established: exogenous GA_3 promotes flowering in chrysanthemum[7], lily[8], and *Paphiopedilum* orchids—where it mediates photoperiod-dependent scape elongation and floral commitment[9]—while in rice, GA_3 modulates submergence-adaptive internode elongation via biosynthetic flux and receptor signaling[10]. Molecularly, core GA pathway components—including the GA INSENSITIVE DWARF1 (GID1) receptor, DELLA repressors, and Phytochrome Interacting Factor (PIF) transcription factors—form a conserved regulatory module[11,12], as seen in lettuce, where the DELLA protein *LsRGL1* controls scape elongation and flowering time via GA pathway regulation[13], highlighting the evolutionary adaptability of GA-driven growth-development coordination.

Studies in pea (*Pisum sativum* L.) have demonstrated that the auxin indole-3-acetic acid (IAA) promotes internode elongation through its regulatory effect on bioactive GA biosynthesis[14]. Concurrently, auxin orchestrates diverse developmental processes, such as cell elongation, organogenesis, and floral stem growth, with conserved regulatory roles across species[15]. In flowering Chinese cabbage, IAA coordinates signaling and transport to regulate internode expansion[16], while in peas, auxin directly induces internode elongation[17]. The auxin pathway, comprising TIR1 receptors, AUX/IAA repressors[18], and auxin response factor (ARF) transcription factors[19], dictates phytohormone function: TIR1 and AUX/IAA drive bolting in *Saposhnikovia divaricata*[20], and *arf6/8* mutants exhibit stem growth defects, underscoring their necessity for inflorescence development[21,22]. Notably, the role of auxin in regulating scape elongation and anthesis in *Clivia miniata* remains uncharacterized.

C. miniata (Amaryllidaceae) is an understory species endemic to South African that has gained commercial prominence as an ornamental plant, especially in China, where it is traditionally associated with prosperity during the Lunar New Year celebrations[23]. However, its unpredictable flowering phenology, which is governed by complex genetic and environmental interactions, poses substantial challenges in horticulture[24]. Current flowering control methods, including exogenous hormone application and temperature manipulation, remain suboptimal[25]. Building on previous work identifying scape elongation as a key developmental checkpoint before anthesis[25], with the aim of screening effective hormones for regulating its flowering anthesis and further exploring effective regulatory measures, this study systematically explored the hormone profile during different stages of scape elongation in *C. miniata*. It demonstrated the regulatory roles of GA and auxin (IAA) in scape elongation through their systematic application. These findings contribute both to a fundamental understanding of hormonal regulation in monocot flowering and to the development of practical

strategies for controlling the reproductive timing of this economically critical ornamental species.

Materials and Methods

Plant materials

C. miniata plants were cultivated in chambers with a controlled environment at Shenyang Agricultural University (41°49' N, 123°34' E). Plants were grown in 27 cm × 25 cm × 25 cm containers filled with an optimized growth medium (3:1:1 leaf mold : coconut chaff : compost, v/v/v; pH 6.0–6.5). The environmental parameters included a 10 h light/14 h dark photoperiod with a 20/10 °C thermoperiod and 65%–75% relative humidity. For metabolomic analyses, scapes with inflorescences were sampled from multiple plants at synchronized developmental time points. Four developmental stages were selected for analysis: the flower bud stage (CM_F), the inflorescence stage (CM_I), the inflorescence emergence stage (CM_E), and the scape stage (CM_S) (Fig. 1a). Triplicate biological replicates (entire scapes with inflorescences) were collected at synchronized time points in each stage, immediately flash-frozen in liquid nitrogen (within 30 s), and stored at −80 °C until liquid chromatography tandem mass spectrometry (LC-MS/MS) analysis.

Microscopic observations

The scape samples underwent standardized histological processing: aseptic aqueous rinsing followed by formalin-acetic acid-alcohol (FAA) chemical fixation. The embedded specimens were sectioned with a microtome at 8 μm thickness following the standard paraffin protocols. The sections were stained with Mayer's hematoxylin, mounted with neutral gum, and imaged using a Leica RM2255 microtome system (Leica Biosystems) equipped with an Olympus DP27 digital camera. Morphometric measurements were performed on high-resolution digital images.

Metabolome assay

Fresh tissue samples (50 mg) from each developmental stage (CM_F, CM_I, CM_E, and CM_S) were cryo-pulverized in 1 mL of an ice-cold extraction buffer (methanol : water : formic acid, 15:4:1 v/v/v) containing 2 μL of stable isotope-labeled internal standards (100 ng/mL). After vortexing (10 min, 25 °C) and centrifugation (14,000 × *g*, 5 min, 4 °C), the supernatants were filtered (0.22-μm nylon mesh) and analyzed by LC-MS/MS (Agilent 6495C QqQ) with the samples maintained at 4 °C during acquisition.

Metabolite profiling was performed on a hyphenated ultrahigh-performance liquid chromatography–electrospray ionization-tandem mass spectrometry (UHPLC-ESI-MS/MS) platform (ExionLC AD UHPLC coupled with a QTRAP 6500+ hybrid triple quadrupole/linear ion trap, Sciex, Shanghai). Chromatographic separation was performed using an ACQUITY UPLC HSS T3 C18 reversed-phase analytical column (100 mm × 2.1 mm inner diameter, 1.8 μm; Waters) under thermostatic conditions (40 °C), with 2-μL injection volumes. A binary solvent system of 0.04% (v/v) acetic acid in water (Phase A) and 0.04% acetic acid in acetonitrile (Phase B) was used at a flow rate of 350 μL/min. A seven-step multisegment gradient was optimized: 2% B (0–1 min), linear ramping to 95% B (1–8 min), isocratic elution (8–9 min), and re-equilibration to the initial conditions (9–12 min).

The QTRAP 6500+ hybrid triple quadrupole–linear ion trap mass spectrometer (Sciex), equipped with a Turbo V electrospray source and operated in polarity-switching mode at ±5,500 V, was calibrated by conducting iterative assessments of the ion suppression effects. The critical ionization parameters included 35 psi of the curtain gas (N_2), 550 °C as the source temperature, and dual nebulizer/auxiliary gases at 35 psi each. Time-scheduled multiple reaction monitoring (MRM) acquisition (dwell time: 50 ms) monitored 214 precursor–product ion pairs for 32 phytohormone subclasses, with the declustering potentials (65–120 V) and collision energies (15–35 eV) dynamically optimized by compound-specific tuning. Raw spectral data processing was performed using Analyst 1.6.3 acquisition software with Multiquant 3.0.3 validation algorithms, implementing peak-area normalization against deuterated internal standards and matrix-matched calibration curves ($R^2 > 0.998$).

Metabolomic data processing was performed using an XCMS-based computational pipeline[26] for chromatographic peak alignment, feature extraction, intensity-based normalization, spectral

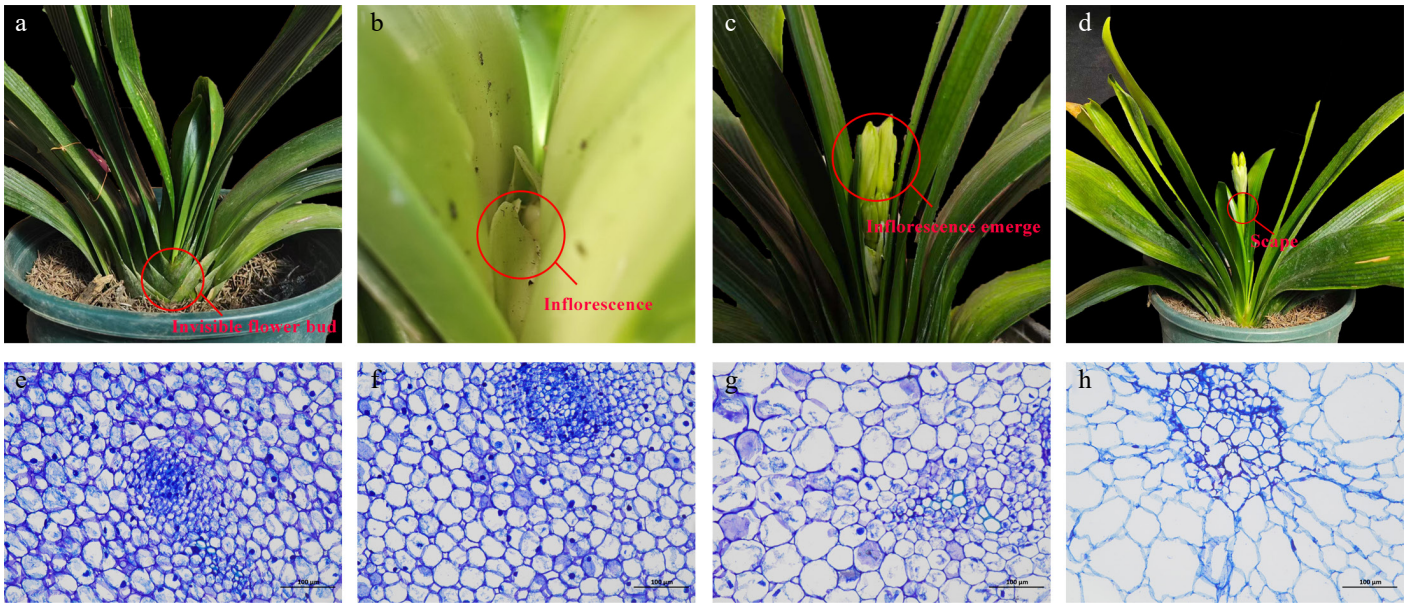

Fig. 1 The four developmental stages before anthesis (a–d) and their corresponding paraffin sections (e–h) of *C. miniata*. (a), (e) Flower bud stage, CM_F, in which the flower bud is invisible. (b), (f) Inflorescence stage, CM_I, when the flower bud develops into a complete inflorescence but both the flower bud and inflorescence are invisible. (c), (g) Inflorescence emergence stage, CM_E, when the inflorescence is visible but the scape is invisible. (d), (h) Scape stage, CM_S, when the scape elongates and both the inflorescence and scape are visible.

deconvolution, and putative metabolite annotation. Multivariate pattern recognition via principal component analysis (PCA) was performed using OriginPro 2022 (OriginLab Corporation, USA) with feature scaling to unit variance prior to eigen decomposition. Metabolites were identified using MetaX[27] with mass accuracy thresholds of < 2 parts per million (ppm) against the Kyoto Encyclopedia of Genes and Genomes (KEGG) database and the Human Metabolome Database (HMDB). Differentially abundant metabolites were defined by a fold change of > 2 or < 0.5 with Benjamini–Hochberg adjusted $p < 0.05$. Correlation networks were visualized using Cytoscape 3.9.1[28] to construct weighted interaction graphs from Pearson's correlation matrices ($|r| > 0.95$, $p < 0.05$).

Hormone treatments applied

Uniform 4-year-old *C. miniata* plants were selected for exogenous hormone application in the greenhouse at Shenyang Agricultural University. At the beginning of the treatment, *C. miniata* plants were at the CM_I stage. Treatment groups included the control (CK, distilled water), GA_3 (50, 100, 150, and 200 mg/L), and IAA (50, 100, 150, and 200 mg/L). Each treatment group included 10 biological replicates. Hormone solutions (1 L per treatment) were applied to the soil for root absorption at the treatment's initiation (1 October 2024), followed by subsequent applications every 10 d until 30 November 2024. Phenological stages—specifically inflorescence emergence and anthesis—were monitored throughout the treatment period (Supplementary Table S1).

Quantitative reverse transcription-polymerase chain reaction

Total RNA isolated from biological specimens (1 μg input) was subjected to first-strand cDNA synthesis employing a gDNA-eliminating PrimeScript RT reagent kit with gDNA removal (TaKaRa Bio, China). Synthesized cDNA was normalized to 200-μL working stocks through spectrophotometric quantification (ratio of absorbance at 260 nm and at 280 nm [A_{260}/A_{280}] = 1.8–2.0) to ensure the template's uniformity for quantitative reverse transcription–polymerase chain reaction (qRT-PCR) validation across experimental replicates. Conserved regions of selected differentially expressed genes were amplified using primers designed with Primer3Web (v4.1.0, https://primer3.ut.ee). All primers used in this study are listed in Supplementary Table S2. A TaqMan Universal SYBR qPCR Master Mix Real-Time PCR system (Vazyme, Nanjing) was used for gene quantitative detection, with *18S rRNA* serving as the internal reference gene[29]. Each group included three technical replicates and three biological replicates. Relative gene expression was calculated using the $2^{-\Delta\Delta C_T}$ method[30]. Statistical significance was assessed by one-way analysis of variance (ANOVA) followed by Tukey's post hoc test. Quantitative traits are presented as the mean ± standard deviation ($n = 5$ biological replicates), and data were visualized using GraphPad Prism 8.0.2 (GraphPad Software, USA) with optimized perceptual color mapping for scientific clarity.

Statistical analysis

All analyses were visualized with GraphPad Prism version 8.0.2 software (San Diego, California, USA). All data of the treatments are expressed as the mean ± standard deviation. Data were analyzed using one-way ANOVA, and the differences were measured using Duncan's test ($p < 0.05$) within GraphPad Prism.

Results

Cell characteristics during scape elongation in *C. miniata*

First, the preflowering developmental process of *C. miniata* was observed. The flower bud differentiation stage was invisible, as the bud remained embedded at the base of the pseudobulb. In a previous study, we performed detailed observations of the flower bud differentiation stage (CM_F). At this time, the flower bud was invisible (Fig. 1a)[25]. Once floral organ development was completed, the inflorescence was formed, marking the inflorescence stage (CM_I). At this stage, the scape had not yet started to elongate and the inflorescence was invisible. However, when we stripped away the leaves, a fully developed inflorescence could be observed (Fig. 1b). Then the scape began to elongate and ejected the inflorescence of the leaves, which was marked as the inflorescence emergence stage (CM_E). At this stage, the inflorescence was visible and the scape was invisible (Fig. 1c). As elongation continued, the plant entered the scape stage (CM_S) and the leaves emerged, eventually leading to anthesis. At this stage, both the inflorescence and scape were visible (Fig. 1d). Paraffin sections prepared from the four developmental stages (CM_F, CM_I, CM_E, and CM_S; Fig.1e–h) revealed coordinated cellular changes associated with scape elongation. A proportional expansion in both the transverse and longitudinal directions was demonstrated, indicative of regulated anisotropic growth. Microscopic analysis showed progressive enlargement and elongation of the parenchyma cells, consistent with the observed macroscopic growth patterns.

Qualitative and quantitative analyses of hormone metabolomics

This study identified and quantified 60 hormones across 8 major classes: 16 cytokinins (CKs), 14 auxins, 12 GAs, 11 jasmonates (JAs), 4 salicylic acids (SAs), 1 ABA, 1 ethylene (ETH), and 1 melatonin (MLT). Normalized hormone content data were visualized via heatmaps (Fig. 2a). Salicylic acid 2-O-β-glucoside, 2-methylthio-cis-zeatin riboside, 6-benzyladenosine, and dihydrozeatin-O-glucoside riboside were exclusively detected in the CM_F stage, coinciding with the completion of flower bud differentiation. These hormones are likely to have a minimal influence on subsequent scape elongation.

PCA was used to assess the overall hormonal differences among developmental phases and to evaluate variability within groups to investigate natural variations in hormone profiles across various scape elongation stages. The analysis revealed distinct hormonal profiles among the four stages (CM_F, CM_I, CM_E, and CM_S), with minimal intrastage variation, thus demonstrating strong sample reproducibility (Fig. 2b). Intergroup and intragroup correlation analyses revealed high consistency among biological replicates within each stage. CM_S, CM_I, and CM_E exhibited significant correlation compared with CM_F, possibly reflecting the unique physiological state of CM_F. This represented the flower bud differentiation phase prior to scape elongation (Fig. 2c).

Analysis of differentially expressed hormones

Hormones exhibiting a fold change of ≥ 1 or ≤ 0.5, with a false discovery rate (FDR) of < 0.05, were classified as differentially expressed. The analysis identified 52 hormones with significant variations across the four developmental stages, comprising 13 auxins, 12 CKs, 11 GAs, 10 JAs, 3 SAs, 1 MLT, 1 ETH, and 1 ABA. Comparative analysis revealed that 10, 11, and 8 hormones were upregulated, whereas 30, 31, and 35 were downregulated in CM_I vs CM_F, CM_E vs CM_F, and CM_S vs CM_F, respectively (Fig. 3a). A Venn diagram identified 20 common differentially expressed hormones across all comparisons, comprising seven JAs, four auxins, three GAs, three CKs, and three SAs (Fig. 3b). A heatmap illustrating the normalized expression profiles of these 20 hormones is presented in Fig. 3c. Correlation network analysis among the 20 analyzed hormones was performed to systematically explore potential interactions. Nodes represented individual hormones, and edges indicated statistically significant ($p < 0.05$) metabolic correlations. Positive correlations

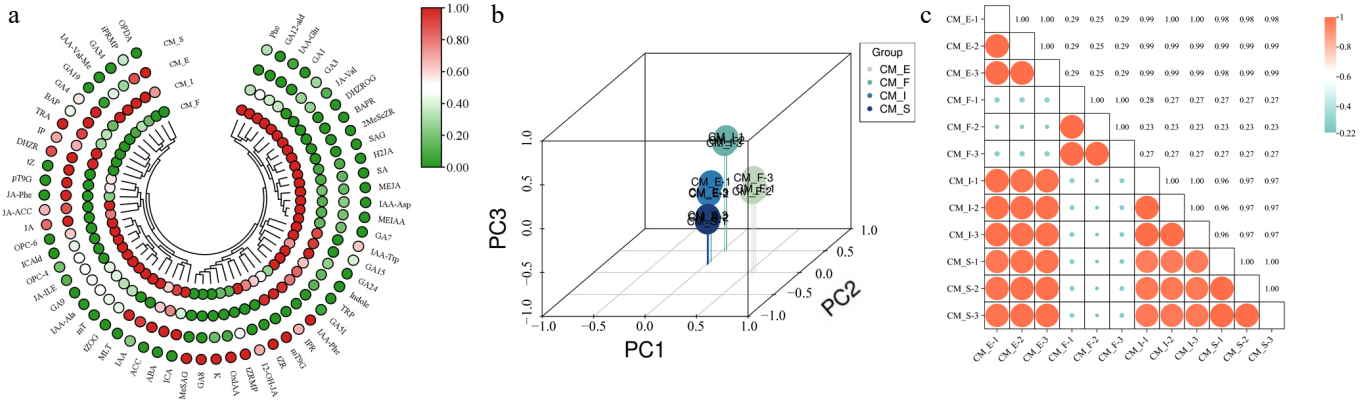

Fig. 2 Quality control analysis of hormone metabolomics in different stages of scape elongation in *C. miniata*. (a) Heatmap of hormone metabolites. (b) PCA score plot. (c) Pearson correlation matrix of phenotypes.

predominated over negative interactions in these networks. The network analysis revealed that IAA-aspartate (IAA-Asp) emerged as the most interconnected node, suggesting its potential role as a central hormonal regulator. Methyl ester IAA (MEIAA) also showed strong co-regulation patterns, particularly with GA_7, indicating its functional association in the hormonal network (Fig. 3d).

The line chart (Fig. 4) clearly demonstrates the content changes in the four auxins, including indole-3-carboxaldehyde (ICAld), IAA-Asp, indoleacetyl glutamic acid (IAA-Glu and MEIAA); three GAs, including GA_1, GA_3, and GA_7; three CKs, including dihydrozeatin-O-glucoside riboside (DHZROG), trans-zeatin-O-glucoside (tZOG), and meta-topolin (mT); seven JAs, including 3-oxo-2-(2-[Z]-pentenyl) cyclopentane-1-butyric acid (OPC-4), jasmonoyl-L-isoleucine (JA-ILE), dihydrojasmonic acid (H2JA), methyl jasmonate (MEJA), 12-hydroxyjasmonic acid (12-OH-JA), N-[(-)-Jasmonoyl]-(L)-valine (JA-Val), 3-oxo-2-(2-[Z]-pentenyl)cyclopentane-1-hexanoic acid (OPC-6); and three SAs, including L-phenylalanine (Phe), salicylic acid (SA), and salicylic acid 2-O-β-glucoside (SAG) during the scape elongation stage. The findings revealed significant upregulation of IAA-Asp, GA_3, OPC-4, JA-Ile, H2JA, JA-Val, OPC-6, and SA levels from the CM_I to the CM_E stage, which coincided with the rapid elongation of the scape.

Promotion of anthesis by exogenous GA_3 and IAA application

GAs and auxins (IAA) play pivotal regulatory roles in floral transition, with exogenous applications of GA_3 and IAA extensively employed in anthesis research. Treatment with both GA_3 and IAA significantly advanced the inflorescence emergence stage, scape elongation, and anthesis date of *C. miniata*, with varying degrees of effect (Tables 1, 2 & Fig. 5). Notably, treatment with 150 mg/L IAA and 100 mg/L GA_3 exhibited the most pronounced promotion of individual inflorescence emergence, advancing the event by 31 and 29 d relative to the control, respectively. Notably, the earliest scape emergence and flowering phenology were induced by 150 mg/L IAA and 100 mg/L GA_3, with 200 mg/L IAA and 150 mg/L GA_3 as suboptimal treatments. However, scape emergence rates were universally decreased across all treatments except 50 mg/L IAA, with 150 mg/L IAA and 150 mg/L GA_3 exhibiting the highest rate at 90%. Further, 100 mg/L IAA and 100 mg/L GA_3 advanced anthesis by 34 and 38 d, respectively. Collectively, our analyses identified 150 mg/L IAA and 200 mg/L GA_3 as the optimal treatment concentrations for promoting early anthesis in *C. miniata*.

Validation of related genes' expression through GA and IAA treatments

RT-qPCR analysis was performed to quantify the transcriptional dynamics of key components in GA and auxin signaling pathways across scape tissues treated with various concentrations of phytohormones to elucidate the molecular mechanisms underlying hormonal regulation (Fig. 6). Specifically, the key genes involved in GA signal transduction were examined, including *CmGID1* (a nuclear receptor of GA signalling[29]), *CmSLR1* (a DELLA protein, repressor of GA signalling[30]), and *CmPIF3* (a transcription factor downstream from DELLA proteins[31]), as well as those in the IAA signal transduction pathway, such as *CmAUX/IAA10* (a auxin transcription factor [TF] repressor), *CmARF1*, *CmARF4*, *CmARF11*, and *CmARF18* (auxin signal TFs downstream of AUX/IAA). The coding DNA sequence data were derived from transcriptome sequencing of *C. miniata* performed in the authors' laboratory and presented in previously unpublished findings.

RT-qPCR analysis revealed a significant induction of auxin response factors, with *CmARF1*, *CmARF4*, *CmARF11*, and *CmARF18* exhibiting marked upregulation in response to both moderate (50 mg/L) and elevated (150 mg/L) IAA concentrations. Similarly, *CmAUX/IAA10* expression was upregulated after exposure to 50 and 100 mg/L IAA, although only the change observed under the 50 mg/L IAA treatment was statistically significant. In contrast, treatment with 150 and 200 mg/L GA resulted in substantially upregulated expression of *CmGID1* and *CmPIF3*. The expression of *CmSLR1*, a DELLA protein, was downregulated following treatment with 150 mg/L GA.

These findings collectively suggest that the exogenous application of GA and IAA triggers distinct responses in their respective signal transduction pathways. The differential expression patterns of *CmAUX/IAA10*, *CmARF1*, *CmARF4*, *CmARF11*, *CmARF18*, *CmGID1*, *CmSLR1*, and *CmPIF3* suggest their potential roles in regulating the differential accumulation of IAA and GA during scape elongation.

Discussion

Cellular differentiation has been established as a crucial determinant of stem elongation in the family Brassicaceae, including economically important species such as *Brassica juncea* and *B. oleracea*[32]. Building on this foundation, the present study systematically characterized four consecutive developmental stages in *C. miniata*: (1) the flower bud differentiation stage (CM_F), (2) the inflorescence stage (CM_I), (3) the inflorescence emergence stage (CM_E), and (4) the scape elongation stage (CM_S). The histomorphometric analysis of paraffin-embedded scape sections demonstrated stage-dependent cellular elongation patterns directly correlating with macroscopic scape growth (Fig. 1). These findings revealed a conserved mechanism coordinating cellular differentiation with organ-level growth dynamics during scape elongation.

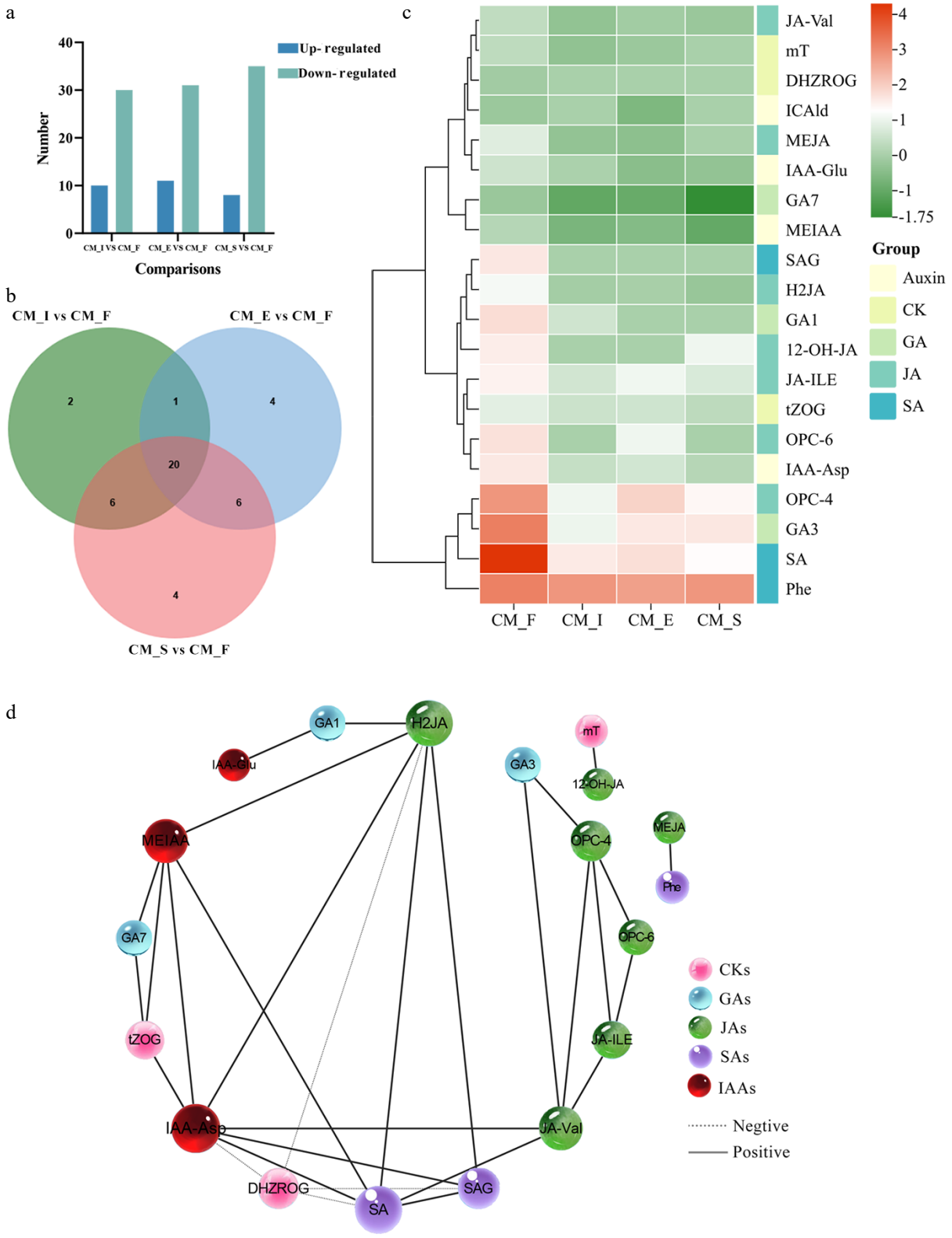

Fig. 3 Overview of differentially expressed metabolites. (a) Pairwise comparisons of different stages. Blue and green bars represent differentially upregulated and downregulated metabolites, respectively. (b) Venn diagrams highlighting different comparisons. (c) A heatmap of 20 differentially expressed hormones. (d) A hormone correlation network analysis of 20 differentially expressed hormones based on Pearson's correlation coefficients ($|r| > 0.95$, $p < 0.05$). The dotted lines between two metabolites represent negative correlations, and the solid lines between two metabolites represent positive correlations. The width of the line between two metabolites changes with the size of the correlation *r*: The thinner the line, the smaller the correlation.

Plant metabolomics has emerged as a powerful tool for elucidating the metabolic networks governing developmental processes[33]. Specifically, scape growth and flowering are precisely controlled by dynamic phytohormone interactions. Comparative metabolomics of early-bolting *Angelica sinensis* cultivars revealed ABA accumulation as a crucial factor regulating flowering time[34]. Complementary

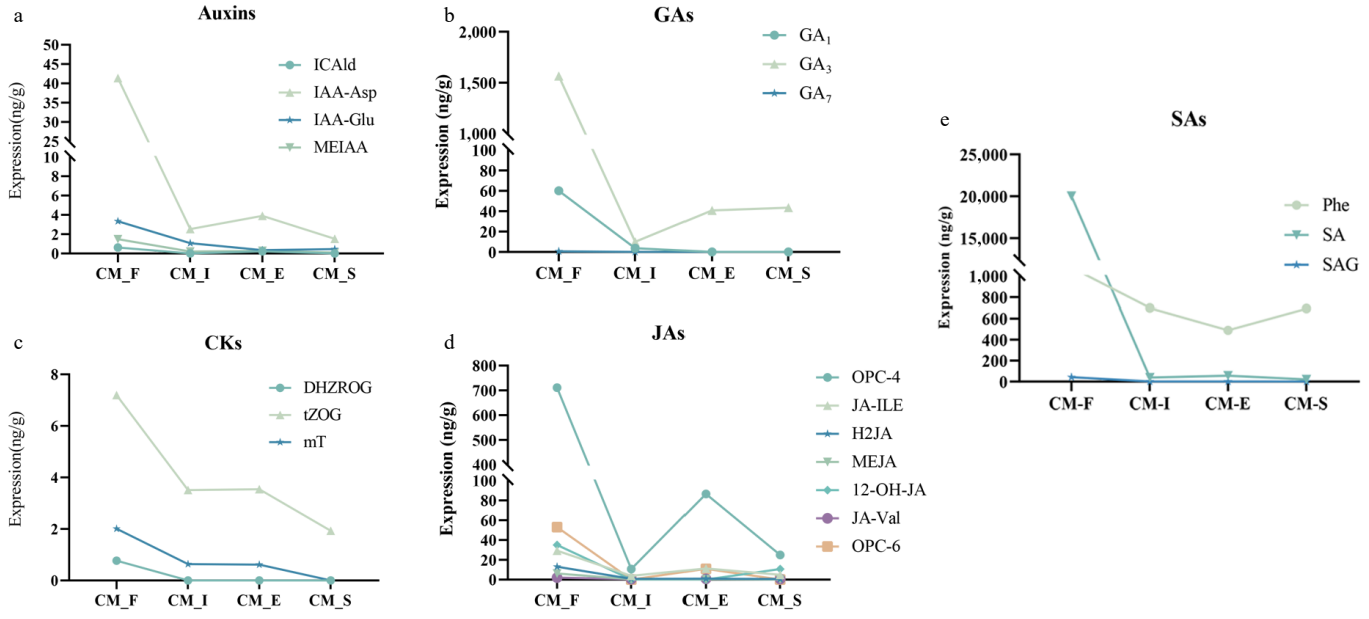

Fig. 4 The expression trend charts of five hormone categories. (a) IAA, auxins; (b) GAs, gibberellins; (c) CKs, cytokinins; (d) JAs, jasmonates; (e) SAs, salicylic acids.

Table 1. Statistics of critical developmental stages for *C. miniata* treated with different concentrations of IAA in 2025.

IAA concentration (mg/L)	Date of inflorescence emergence (month/day)	Date of scape elongation (month/day)	Date of anthesis (month/day)	Days of advanced anthesis (days)	Rate of scape emergence (%)
0 (control)	2/2 ± 0.5	2/15 ± 0	2/26 ± 0.5	0c	100.0
50	1/17 ± 0.5	1/26 ± 0.5	2/12 ± 0.5	14.21 ± 3.59b	100.0
100	1/16 ± 0.5	1/25 ± 0.5	1/23 ± 0.5	34.19 ± 0.97a	20.0
150	1/1 ± 0.5	1/14 ± 0.5	1/28 ± 0.5	29.81 ± 3.52a	90.0
200	1/6 ± 0.5	1/22 ± 0.5	2/2 ± 0.5	24.15 ± 2.12a	60.0

Different lowercase letters in the column indicate statistically significant differences ($p < 0.05$) as determined by Duncan's multiple range test.

Table 2. Statistics of critical developmental stages in *C. miniata* treated with different concentrations of GA_3 in 2025.

GA concentration (mg/L)	Date of inflorescence emergence (month/day)	Date of scape elongation (month/day)	Date of anthesis (month/day)	Days of advanced anthesis (days)	Rate of scape emergence (%)
0 (control)	2/2 ± 0.5	2/15 ± 0	2/26 ± 0.5	0c	100.0
50	1/5 ± 0.5	1/18 ± 0.5	1/22 ± 0.5	35.15 ± 3.59a	50.0
100	1/3 ± 0.5	1/9 ± 0.5	1/19 ± 0.5	38.31 ± 0.97a	50.0
150	1/9 ± 0.5	1/18 ± 0.5	2/1 ± 0.5	25.33 ± 1.52b	90.0
200	1/4 ± 0.5	1/10 ± 0.5	1/22 ± 0.5	35.81 ± 3.52a	80.0

Different lowercase letters in the column indicate statistically significant differences ($p < 0.05$) as determined by Duncan's multiple range test.

studies in *Hylomecon japonica* demonstrated that vernalization-induced floral transition was accompanied by a decrease in IAA levels and an increase in the GA_3/ABA ratio[35]. These findings underscore the conserved role of hormone homeostasis in plants' reproductive development. This study profiled hormones across four developmental stages (CM_F, CM_I, CM_E, and CM_S) in *C. miniata* to decipher the regulatory network governing scape elongation. For this purpose, 52 differentially expressed hormones were identified, elucidating the underlying mechanisms of scape elongation in this ornamental species. This study detected 20 conserved differentially expressed hormones among the three pairwise comparisons (CM_I vs CM_F, CM_E vs CM_F, and CM_S vs CM_F). The predominant hormonal classes included JAs, auxins, GAs, CKs, and SAs, suggesting their central regulatory functions. An especially remarkable finding was the consistently high expression of L-Phe throughout flower bud differentiation and scape elongation, indicating its potential involvement in hormone biosynthesis, which is crucial for developmental progression. The network analysis of hormone correlations identified IAA-Asp as a central hub within the network. The strong correlation between MEIAA and GA_7 implies substantial crosstalk between the auxin and GA pathways, potentially coordinating growth processes during scape elongation. Overall, these findings significantly enhance the understanding of the hormonal regulation of scape elongation.

The transition to flowering in plants is precisely regulated by complex molecular networks integrating internal developmental cues with external environmental signals[36]. GAs serve as central regulators of this process, coordinating reproductive timing across diverse species[37,38]. The key findings establish the regulatory role of GA in stem elongation. GA_3-induced stem elongation is reversibly inhibited by chlorocholine chloride-mediated suppression of GA biosynthesis in *Brassica napus*[39]. Exogenous GA application directly modulates stem elongation kinetics in *Triticum aestivum*[40]. Previous studies demonstrated the fundamental role of GA in

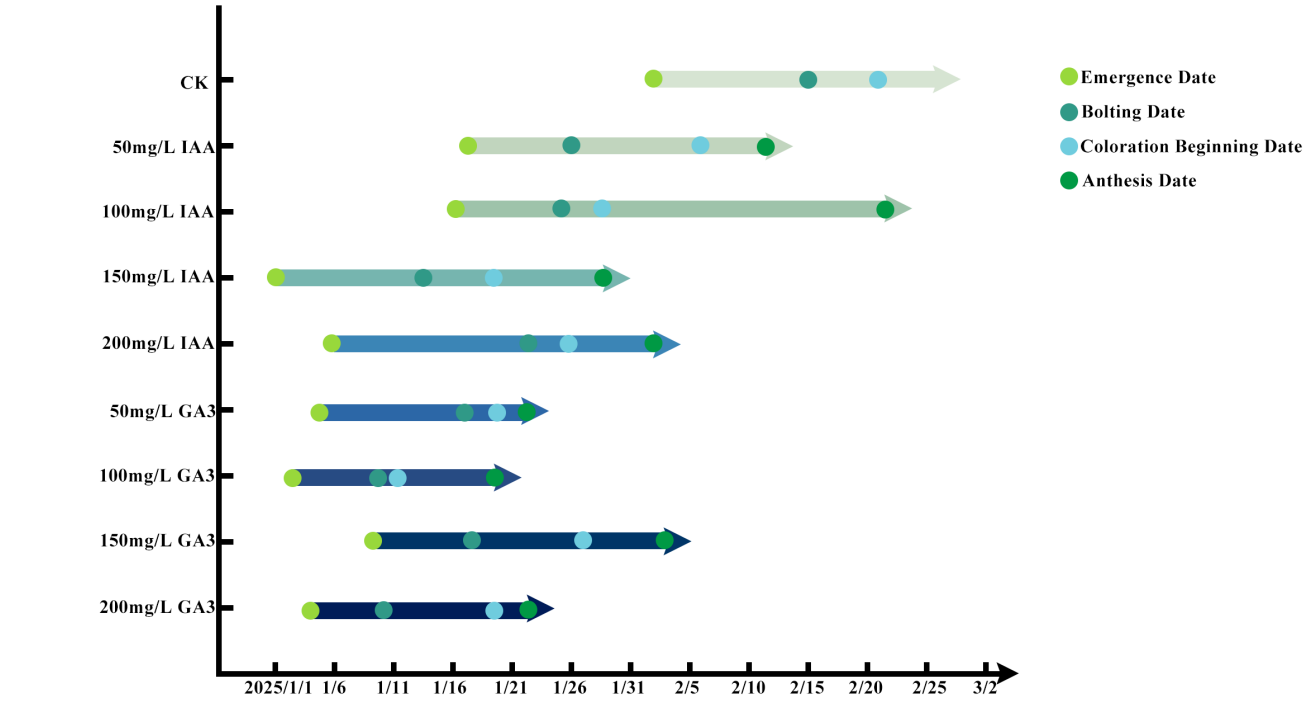

Fig. 5 Timeline of inflorescence emergence, scape elongation, color onset, and anthesis in *C. miniata* under different treatments.

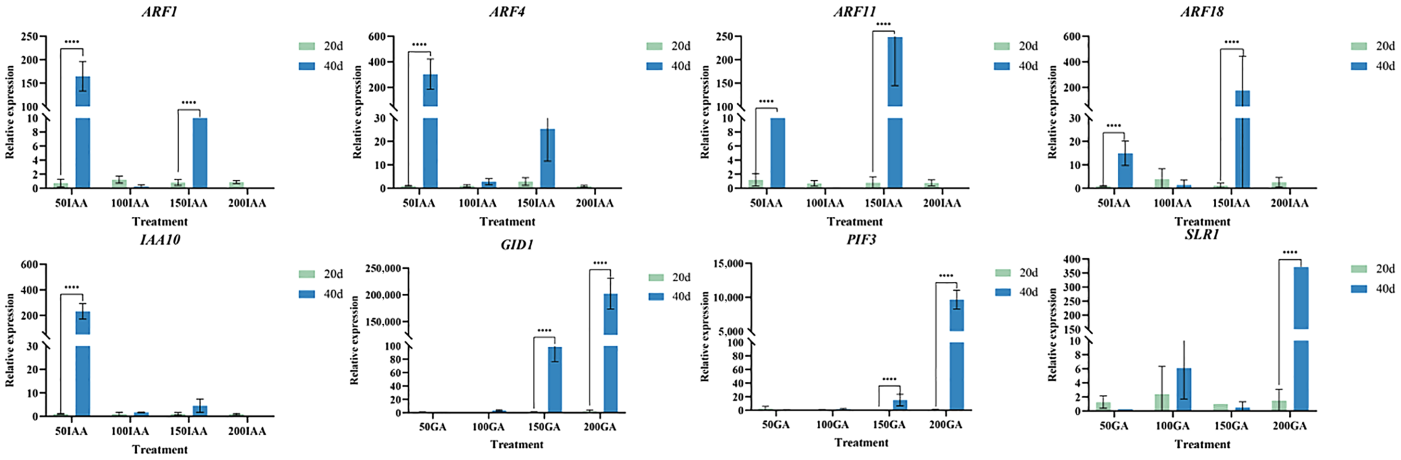

Fig. 6 Relative expression of scape elongation-related genes after different treatments. Error bars = standard deviation. **** $p < 0.01$ (Student's *t*-test).

regulating the developmental progression to flowering through stem growth modulation. In the present study, the expression dynamics of GA_3 exhibited a distinct temporal pattern in *C. miniata*. The expression levels began to rise in the CM_I stage and peaked in the CM_E stage. This expression pattern indicated the involvement of GA_3 in the early phases of scape development, particularly in scape elongation. A controlled dose-response experiment was conducted using 10 plants per treatment group to further clarify the role of GA_3. This was followed by foliar applications of 50–200 mg/L GA_3. The 100 and 200 mg/L treatments led to the earliest scape emergence, compared with the control plants, which showed a 1-month delay. The 100 mg/L treatment advanced anthesis by 38 d, corroborating the authors' previous findings[25] and validating the role of GA_3 in promoting flowering in *C. miniata*. Disruptions in GA signaling components often result in abnormal flowering phenotypes. The GA signaling pathway is regulated by an evolutionarily conserved GID1-DELLA module. However, F-box proteins display lineage-specific divergence, with *At*SLY1 functioning in *A. thaliana* and *Os*GID2 in *O. sativa*[40]. Bioactive GA isoforms form ternary complexes with GID1 and DELLA proteins. This interaction triggers the polyubiquitination of DELLA proteins by Skp, Cullin, F-box containing (SCF) complex E3 ligases, followed by their proteasomal degradation, thereby activating the expression of GA-responsive genes[41–43]. This process regulates stem elongation and reproductive transitions through hierarchical cascades of phosphorelay signaling[13]. PIFs regulate flowering in both *Phalaenopsis* and Chinese pine by integrating GA signaling through direct interactions with DELLA proteins[12,44]. An investigation of GA signaling components in *C. miniata* revealed a significant upregulation of *CmGID1* expression at the onset of scape elongation in all GA-treated groups compared with the controls. Additionally, treatment with 150 and 200 mg/L of GA led to substantially upregulated expression of *CmPIF3*. The consistent induction of *CmGID1* and *CmPIF3* suggests their potential role as positive regulators of scape elongation in *C. miniata*.

The auxin class of phytohormones orchestrates essential developmental processes, from embryogenesis to tropic responses[45]. IAA, the primary active auxin synthesized in apical meristems, regulates

stem elongation in various species, including *Narcissus pseudonarcissus* and *Paeonia suffruticosa*[46]. Although exogenous IAA accelerates bolting in *Lactuca sativa*[47], the metabolomic analysis of *C. miniata* in this study identified two distinct auxin derivatives as the key scape elongation regulators: MEIAA and IAA-Asp. These findings revealed species-specific adaptations in auxin-mediated growth regulation while maintaining the conserved role of hormones in developmental control.

Systematic dose-response experiments were conducted, applying 50–200 mg/L IAA. Specifically, the 150 mg/L IAA treatment proved most effective in promoting early inflorescence emergence. In contrast, control plants exhibited a delay in scape emergence of approximately 1 month compared with the plants in the treatment groups. Although the 50 mg/L IAA treatment yielded emergence rates equivalent to those of the controls (100%), all treatment concentrations accelerated anthesis. The 100 mg/L IAA treatment had the most pronounced effect, advancing anthesis by 34 d. These results establish a concentration-dependent function of exogenous IAA in regulating the anthesis time of *C. miniata*. The findings can significantly enhance the understanding of auxin-mediated flowering control, particularly in monocot species.

In *A. thaliana*, the auxin signaling pathway is regulated by the TIR1/AFB receptor family. This family facilitates the ubiquitin-dependent degradation of Aux/IAA repressors, thereby initiating the subsequent activation of ARF transcription factors[48–49]. Once activated, the ARFs regulate the expression of auxin-responsive genes, including members of the Aux/IAA and GH3 families as their transcriptional targets[50]. Similarly, in *L. sativa,* several ARF homologs, such as *LsARF2, LsARF3*, and *LsARF8a*, mediate auxin responses[51,52]. This conservation of the auxin signaling pathway across various plant species underscores its fundamental significance in plant biology. The present study on auxin signaling in *C. miniata* revealed that IAA upregulated *AUX/IAA10* expression. Additionally, the exogenous application of 50 and 150 mg/L IAA led to increased expression of multiple *CmARF* genes (*CmARF1*, *CmARF4*, *CmARF11*, and *CmARF18*) in scape tissues. These results suggest a role of the components of the auxin signaling pathway in regulating scape elongation. Thus, IAA likely promotes stem growth by activating the transcription of key signaling components.

Conclusions

This study comprehensively elucidated the regulatory mechanisms underlying scape elongation and anthesis in *C. miniata*. By systematically analyzing four developmental stages, the study revealed that scape elongation is a pivotal determinant of anthesis timing, operating independently of flower bud differentiation. The histological analysis clearly linked cellular elongation to scape growth. The metabolomic profiling in this study identified 52 differentially expressed hormones, including 20 conserved regulators such as JAs, auxins, GAs, CKs, and SAs, which together formed a complex regulatory network. The consistent expression of L-Phe throughout development and the identification of IAA-Asp as a central hub in the network underscored their crucial regulatory roles. Functional experiments demonstrated that GA_3 promoted scape emergence and anthesis in a dose-dependent manner. This effect was corroborated by the upregulation of GID1, a key component of the GA signaling pathway. Moreover, the present study revealed that auxin exerted concentration-specific effects on scape development by regulating *AUX/IAA10* and *ARF* genes' expression. Collectively, these findings significantly enhance our understanding of scape development. They also provide a solid framework for future mechanistic studies and offer valuable insights for horticultural strategies to precisely control the time of anthesis.

Author contributions

The authors confirm contributions to the paper as follows: study conception and design, data collection, analysis, and interpretation of results: Ji Y; draft manuscript preparation: Ji Y, Lei J, Xue L; manuscript revision: Lei J, Xue L. All authors reviewed the results and approved the final version of the manuscript.

Data availability

All data generated or analyzed during this study are included in this published article and its supplementary information files.

Acknowledgments

This study was supported by the Basic Scientific Research Project for Universities of the Education Department of Liaoning Province in 2022 (LJKMZ20222130).

Conflict of interest

The authors declare that they have no conflict of interest.

Supplementary information accompanies this paper at (https://www.maxapress.com/article/doi/10.48130/opr-0025-0037)

Dates

Received 5 May 2025; Revised 15 July 2025; Accepted 28 July 2025; Published online 27 October 2025

References

1. Han Y, He Y, Yue S, Guo B, Zhu Q, et al. 2023. Floral bud differentiation and mechanism underlying androdioecy of *Osmanthus fragrans*. *Ornamental Plant Research* 3:11
2. Fukazawa J, Ohashi Y, Takahashi R, Nakai K, Takahashi Y. 2021. DELLA degradation by gibberellin promotes flowering via GAF1-TPR-dependent repression of floral repressors in *Arabidopsis*. *The Plant Cell* 33:2258–72
3. Pouteau S, Albertini C. 2009. The significance of bolting and floral transitions as indicators of reproductive phase change in *Arabidopsis*. *Journal of Experimental Botany* 60:3367–77
4. Gol L, Tomé F, von Korff M. 2017. Floral transitions in wheat and barley: interactions between photoperiod, abiotic stresses, and nutrient status. *Journal of Experimental Botany* 68:1399–410
5. Golz JF, Hudson A. 2002. Signaling in plant lateral organ development. *The Plant Cell* 14:S277–S288
6. Olszewski N, Sun TP, Gubler F. 2002. Gibberellin signaling: biosynthesis, catabolism, and response pathways. *The Plant Cell* 14:S61–S80
7. Sumitomo K, Li T, Hisamatsu T. 2009. Gibberellin promotes flowering of chrysanthemum by upregulating *CmFL*, a chrysanthemum *FLORICAULA/LEAFY* homologous gene. *Plant Science* 176:643–49
8. Li W, Yong Y, Zhang Y, Lyu Y. 2019. Transcriptional regulatory network of GA floral induction pathway in LA hybrid lily. *International Journal of Molecular Sciences* 20:2694
9. Yin Y, Li J, Guo B, Li L, Ma G, et al. 2022. Exogenous GA_3 promotes flowering in *Paphiopedilum callosum* (Orchidaceae) through bolting and lateral flower development regulation. *Horticulture Research* 9:uhac091
10. Nagai K, Kondo Y, Kitaoka T, Noda T, Kuroha T, et al. 2014. QTL analysis of internode elongation in response to gibberellin in deepwater rice. *AoB Plants* 6:plu028
11. Achard P, Gusti A, Cheminant S, Alioua M, Dhondt S, et al. 2009. Gibberellin signaling controls cell proliferation rate in *Arabidopsis*. *Current Biology* 19:1188–93
12. Guo Y, Deng C, Feng G, Liu D. 2024. Genome-wide analysis of phytochrome-interacting factor (PIF) families and their potential roles in light and gibberellin signaling in Chinese pine. *BMC Genomics* 25:1017

13. Wang S, Luo C, Sun L, Ning K, Chen Z, et al. 2022. *LsRGL1* controls the bolting and flowering times of lettuce by modulating the gibberellin pathway. *Plant Science* 316:111175
14. Yang T, Law DM, Davies PJ. 1993. Magnitude and kinetics of stem elongation induced by exogenous indole-3-acetic acid in intact light-grown pea seedlings. *Plant Physiology* 102:717–24
15. Xu RY, Niimi Y, Ohta Y, Kojima K. 2008. Changes in diffusible indole-3-acetic acid from various parts of tulip plant during rapid elongation of the flower stalk. *Plant Growth Regulation* 54:81–88
16. Kou E, Huang X, Zhu Y, Su W, Liu H, et al. 2021. Crosstalk between auxin and gibberellin during stalk elongation in flowering Chinese cabbage. *Scientific Reports* 11:3976
17. Ross JJ, O'Neill DP, Rathbone DA. 2003. Auxin-gibberellin interactions in pea: integrating the old with the new. *Journal of Plant Growth Regulation* 22:99–108
18. Dharmasiri N, Estelle M. 2004. Auxin signaling and regulated protein degradation. *Trends in Plant Science* 9:302–8
19. Leyser O. 2018. Auxin signaling. *Plant Physiology* 176:465–79
20. Zhang M, Wang W, Liu Q, Zang E, Wu L, et al. 2023. Transcriptome analysis of *Saposhnikovia divaricata* and mining of bolting and flowering genes. *Chinese Herbal Medicines* 15:574–87
21. Zhang Y, Nie C, Zhang J, Guo W, Ding P, et al. 2023. A gibberellin-responsive transcription factor from *Phalaenopsis* 'Big Chili' (*PIF4*) promotes flowering in *Arabidopsis thaliana*. *Plant Growth Regulation* 101:361–71
22. Roumeliotis E, Visser RGF, Bachem CWB. 2012. A crosstalk of auxin and GA during tuber development. *Plant Signaling & Behavior* 7:1360–63
23. Collen M, Elizabeth Bosede A, Adebowale Emmanuel A. 2021. *Clivia miniata* (Lindl.) Bosse, (Amaryllidaceae): botany, medicinal uses, phytochemistry and pharmacological properties. *Journal of Applied Pharmaceutical Science* 11:12–18
24. Funnell KA. 2017. Scheduling flowering in *Clivia miniata* Regel for different markets. *Acta Horticulturae* 1171:39–46
25. Ji Y, Zhang H, Wang C, Wang C, Zhao J, et al. 2024. What is going on with the flower bud differentiation and metabolites control of scape elongation on *Clivia miniata* Regel? *Scientia Horticulturae* 324:112626
26. Smith CA, Want EJ, O'Maille G, Abagyan R, Siuzdak G. 2006. XCMS: processing mass spectrometry data for metabolite profiling using nonlinear peak alignment, matching, and identification. *Analytical Chemistry* 78:779–87
27. Wen B, Mei Z, Zeng C, Liu S. 2017. metaX: a flexible and comprehensive software for processing metabolomics data. *BMC Bioinformatics* 18:183
28. Shannon P, Markiel A, Ozier O, Baliga NS, Wang JT, et al. 2003. Cytoscape: a software environment for integrated models of biomolecular interaction networks. *Genome Research* 13:2498–504
29. Li Y, Gao R, Zhang J, Wang Y, Kong P, et al. 2022. The biochemical and molecular investigation of flower color and scent sheds lights on further genetic modification of ornamental traits in *Clivia miniata*. *Horticulture Research* 9:uhac114
30. Livak KJ, Schmittgen TD. 2001. Analysis of relative gene expression data using real–time quantitative PCR and the $2^{-\Delta\Delta CT}$ method. *Methods* 25:402–8
31. Zhao J, Bo K, Pan Y, Li Y, Yu D, et al. 2023. Phytochrome-interacting factor PIF3 integrates phytochrome B and UV-B signaling pathways to regulate gibberellin-and auxin-dependent growth in cucumber hypocotyls. *Journal of Experimental Botany* 74(15):4520–39
32. Zhang YW, Jin D, Xu C, Zhang L, Guo MH, et al. 2015. Regulation of bolting and identification of the α-tubulin gene family in *Brassica rapa* L. ssp. *pekinensis*. *Genetics and Molecular Research* 15:1–13
33. Hall R, Beale M, Fiehn O, Hardy N, Sumner L, et al. 2002. Plant metabolomics: the missing link in functional genomics strategies. *The Plant Cell* 14:1437–40
34. Zhu C, Bai Y, Jiang Y, Zhang Y, Wang S, et al. 2024. Integrated transcriptomic and metabolomic analysis reveals the regulation mechanism of early bolting and flowering in two cultivars of *Angelica sinensis*. *Heliyon* 15:e28636
35. Yan X, Liu J, Wu KX, Yang N, Pan LB, et al. 2022. Comparative analysis of endogenous hormones and metabolite profiles in early-spring flowering plants and unflowered plants revealing the strategy of blossom. *Journal of Plant Growth Regulation* 41:2421–34
36. Cai K, Zhu S, Jiang Z, Xu K, Sun X, et al. 2024. Biological macromolecules mediated by environmental signals affect flowering regulation in plants: a comprehensive review. *Plant Physiology and Biochemistry* 214:108931
37. Teotia S, Tang G. 2015. To bloom or not to bloom: role of microRNAs in plant flowering. *Molecular Plant* 8:359–77
38. Zhang N, Xie YD, Guo HJ, Zhao LS, Xiong HC, et al. 2016. Gibberellins regulate the stem elongation rate without affecting the mature plant height of a quick development mutant of winter wheat (*Triticum aestivum* L.). *Plant Physiology and Biochemistry* 107:228–36
39. Dahanayake SR, Galwey NW. 1999. Effects of interactions between low-temperature treatments, gibberellin (GA_3) and photoperiod on flowering and stem height of spring rape (*Brassica napus* var. *annua*). *Annals of Botany* 84:321–327
40. Itoh H, Ueguchi-Tanaka M, Sato Y, Ashikari M, Matsuoka M. 2002. The gibberellin signaling pathway is regulated by the appearance and disappearance of *SLENDER RICE1* in nuclei. *The Plant Cell* 14:57–70
41. Murase K, Hirano Y, Sun TP, Hakoshima T. 2008. Gibberellin-induced DELLA recognition by the gibberellin receptor GID1. *Nature* 456:459–63
42. Dill A, Thomas SG, Hu J, Steber CM, Sun TP. 2004. The *Arabidopsis* F-box protein SLEEPY1 targets gibberellin signaling repressors for gibberellin-induced degradation. *The Plant Cell* 16:1392–405
43. Harberd NP, Belfield E, Yasumura Y. 2009. The angiosperm gibberellin-GID1-DELLA growth regulatory mechanism: how an "inhibitor of an inhibitor" enables flexible response to fluctuating environments. *The Plant Cell* 21:1328–39
44. Zhao Y. 2010. Auxin biosynthesis and its role in plant development. *Annual Review of Plant Biology* 61:49–64
45. Edelbluth E., Kaldewey H. 1976. Auxin in scapes, flower buds, flowers, and fruits of daffodil (*Narcissus pseudonarcissus* L.). *Planta* 131:285–91
46. Wang Y, Li B, Li Y, Du W, Zhang Y, et al. 2022. Application of exogenous auxin and gibberellin regulates the bolting of lettuce (*Lactuca sativa* L.). *Open Life Sciences* 17:438–46
47. Chen C, Huang W, Hou K, Wu W. 2019. Bolting, an important process in plant development, two types in plants. *Journal of Plant Biology* 62:161–69
48. Yu Z, Zhang F, Friml J, Ding Z. 2022. Auxin signaling: research advances over the past 30 years. *Journal of Integrative Plant Biology* 64:371–92
49. Abel S, Theologis A. 1996. Early genes and auxin action. *Plant Physiology* 111:9–17
50. Hu M, Qi Z, Ren Z, Tong J, Wang B, et al. 2022. Genome-wide analysis of auxin response factors in lettuce (*Lactuca sativa* L.) reveals the positive roles of *LsARF8a* in thermally induced bolting. *International Journal of Molecular Sciences* 23(21):13509
51. Yang X, Jia K, Zhu J, Zhang Y, Tian Y, et al. 2023. Gene characterization and protein expression analysis of *LsARF2* in lettuce (*Lactuca sativa* L.) under high temperature. *Journal of Agricultural Science* 15:42
52. Li Y, Zhu J, Feng Y, Li Z, Ren Z, et al. 2022. LsARF3 mediates thermally induced bolting through promoting the expression of *LsCO* in lettuce (*Lactuca sativa* L.). *Frontiers in Plant Science* 13:958833